



Growth Morphology of Nodular Primary Silicon in Hypereutectic Al–Si Alloy and Its Growth Mechanism

Ruyao Wang and Weihua Lu

Abstract

Microstructure of nodular primary silicon crystal in hypereutectic Al–Si alloy has been metallographically studied. Etched growth traces were used to investigate the growth mechanism of nodular silicon crystal. Silicon nodule as an equiaxed polyhedron faced with different high-index facets grew in concentric growth mode with almost equal growth rate of growth facets. The unequal growth rate between two neighboring facets caused the new high-index facet to appear, making silicon crystal more roundish. The reason for the formation of nodular silicon crystal with multi-facets was discussed in terms of the discrepancy of diffusion rate of silicon atoms in melt and crystallization rate of silicon grain with changes in temperature. In current study, the high cooling rate in freezing of Al-14wt%Si alloy casting treated by the designed modifier consisting of P, Ti, B, and mischmetal (RE) near the chill mould promotes the occurrence of silicon nodule.

Keywords

Al–Si alloy • Nodular silicon crystal • Growth mechanism

Introduction

In the solidification of a hypereutectic Al–Si alloy, the primary phase of faceted Si crystals growing from the melt is known to exhibit a wide variety of morphologies, mostly faced by {111} facets [1, 2]. Initially, five basic morphologies of primary silicon were defined, namely, octahedral,

plate-like hexagonal, equiaxial, star-like, and spheroidal morphologies. Over past decades, a lot of researches have been carried out on the microstructure and growth mechanism of the primary silicon phase in Al–Si alloys [3–14]. However, relatively little work has been focused on the spherical silicon crystal, either its microstructure or growth mechanism. In 1926, Gwyer and Philips have firstly observed the small silicon nodules in Al-16.6wt%Si-0.5wt% Fe alloy treated by 5wt% NaOH [15]. One year later Gayler reported that as silicon content increased to 17.52wt% Si in hypereutectic alloy containing 0.02wt%Na, a few nodular silicon crystals also could have been found [16]. High undercooling achieved by chill casting [17, 18] or droplet levitation [10, 11] is another powerful tool to spheroidize silicon, either primary or eutectic in solidification of alloy. It was found that as undercooling reached 73 °C or more primary silicon transformed from faceted octahedral shape into nonfaceted contour growing in a roundish form [8, 9]. In 1968, M. Day reported that the spherulites are characterized by high twin density and radial twin markings [19]. If the twin density is sufficiently high, the primary silicon can grow in a spherulitic form. This so-called spherical primary silicon is not perfectly spheroidal shape, and is simply a multi-faceted form of the basic polyhedral shape [20]. But the nucleus appears in a number of different form, such as irregular crystal or octahedral AlP crystal in P-treated Al–Si alloy [3, 21]. By now what growth mechanism to develop the spherical silicon is mystery.

As is well known, the growth traces can serve as a powerful tool to understand the varieties of growth morphology of crystal during solidification or heating [22]. In previous studies, authors revealed the growth striations of primary silicon crystal in Al–Si alloys by appropriate etching techniques [3, 21], studying the growth mechanism of octahedral, spinel, star-like, and other irregular external shape of primary silicon phase. The growth striations appear in closed concentric lines from the nucleus to external surface of crystal, marking the external shape of the crystal at

R. Wang (✉) · W. Lu
Institute of Materials Science and Engineering, Donghua University, 1882 West Yan-an Rd., Shanghai, 200051, China
e-mail: ryaowang@163.com

successive stages in its growth from the melt. The spacing between successive growth traces represents the distance of growth in a certain time interval of growth and is proportional to the velocity of growth. An important feature is that the spacing varies with time for different facets, greatly affecting the morphology at certain interval and finally external contour of Si grain. It has been frequently found that one of two neighbors' low-index faces $\{111\}$ grows faster than another, consequently leading to the occurrence of other high-index plane. Therefore, the profile of the crystal approaches an equiaxed shape with different low- and high-index growth facet planes parallel to external habit facets, respectively. This phenomenon raises one question whether the spheroid silicon is the equiaxed polyhedron and how the silicon nodule grows up.

In the work, the aims focus on the following:

- (1) The observation of variety of growth morphology of nodular silicon crystal in hypereutectic Al–Si alloy via growth rates.
- (2) The study of the growth mechanism of nodular silicon.

Experimental Procedure

Metallographic samples were taken from Al-14wt%Si alloy listed in Table 1.

The alloy was melted in an 8-kg graphite crucible placed in an electric resistance furnace. The melt was treated by the designed modifier consisting of P, Ti, B, and mischmetal (RE); degassed with N_2 ; and then poured into metal mould to form a casting $40 \times 50 \times 120$ mm in size. Polished specimens were attached by a hot aqueous solution of 20 wt% NaOH at 80 °C, which dissolved the matrix to leave silicon crystals standing in relief and also etched the growth traces in silicon crystals [21]. Because of the high cooling rate at the boundary of casting near the mould introducing a higher undercooling in solidification [23, 24], a few of roundish primary silicon crystals often appear in specimens [9, 10]. This provides the possibility to study the microstructural characteristics and growth mechanism of nodular silicon crystal in casting. The information about orientation of facets is referred to our previous articles [3, 21].

Observation and Analysis

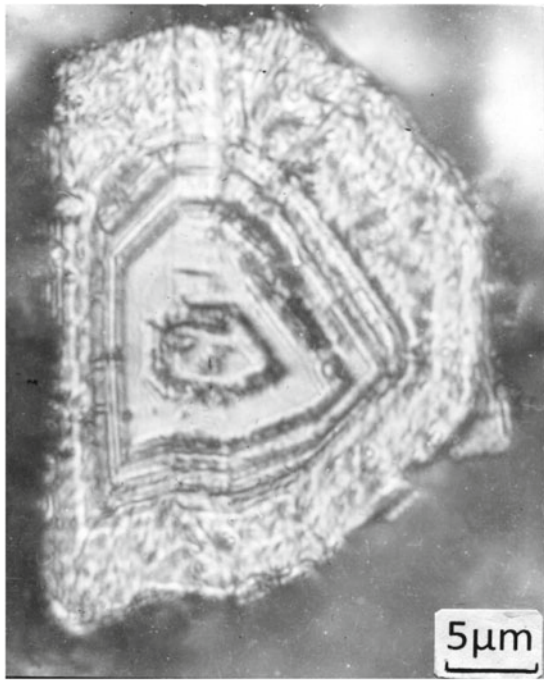
Two stages in growth process are demonstrated by microstructural observation. Firstly, a stem crystal is developed from an octahedral silicon nucleus in initial stage of growth. Then, the stem crystal grows in concentric layer mode; the low-indexed facets gradually grow out, causing a lot of new high-indexed facets to occur. Crystal growth in this mode continues from the center of crystal to the external periphery. A silicon nodule is gradually developed.

Initial Stage of Growth

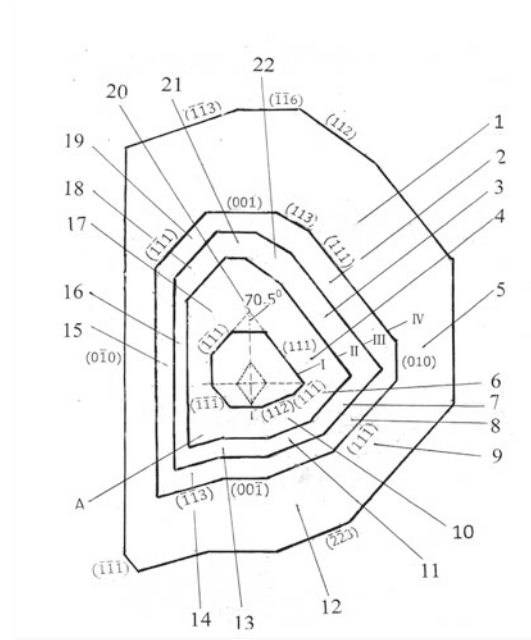
Figures 1 and 2 show images and related crystallographic analyses of semi-nodular and nodular silicon crystal respectively, in which the growth traces revealed by hot etching are clearly displayed. Most series of growth traces appear as closed concentric lines with same growth space in certain intervals similar to a distinct pattern of concentric tree rings. The measurement of angles between growth traces in two nodules yields an interesting event. In stage of growth four growth traces can be found, as shown by dotted line in Figs. 1a and 2a, imposing a flat shape with two pairs of opposite traces parallel, and one pair of opposite angle of 70.5° and other of 109.5° , thus the four growth traces are (111) , $(\bar{1}\bar{1}1)$, $(11\bar{1})$ and $(\bar{1}\bar{1}\bar{1})$, respectively. The plane of the section obviously lies parallel to $\{110\}$ of an octahedron. The orientation of every growth trace can be easily confirmed by angular measurement between traces. Each straight section of growth trace runs parallel to an external surface facet such as $\{111\}$, $\{100\}$, $\{112\}$, and others. In the center of the semi-nodular crystal, a silicon particle exhibits unclear polygonal contour (Fig. 1a). It is interesting that in the early stage of growth an irregular octahedron with many facets, such as $\{111\}$, $\{001\}$, and $\{11\bar{2}\}$, apparently exists as shown in Fig. 1b, c. In our previous study, it was found that the grown morphology of silicon particle is greatly affected by the contour of silicon crystal formed in initial stage [3, 21]. Since phosphorus was used in the designed modifier, it is to be expected that the primary silicon crystal would nucleate heterogeneously. The likely nucleus would be AlP crystal, which has a structure and crystal parameters close to those of silicon [25] Thus, in early growth, a silicon crystal on AlP grows with eight $\{111\}$ triangles. During initial growth from the pyramid silicon crystal

Table 1 Analysis of Al–Si alloys tested wt%

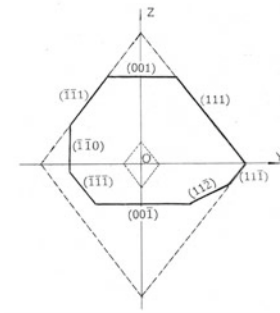
Alloy	Si	Cu	Mg	Mn	Fe
Al-14wt%Si	14.0–14.6	0.90–1.20	0.50–0.55	0.26–0.32	0.35–0.48



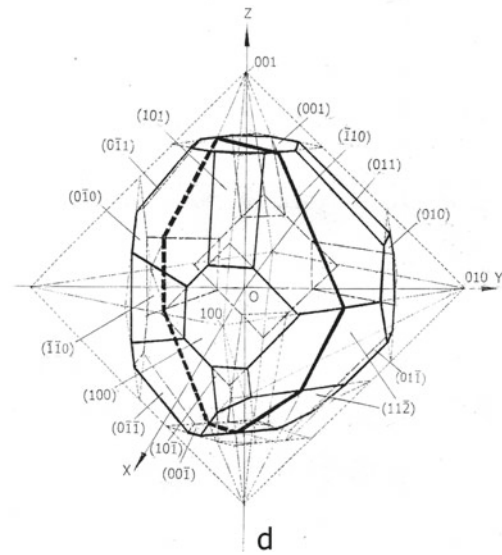
a



b



c



d

Fig. 1 a Cross section (110) through a semi-nodular silicon crystal exhibiting a concentric layer growth traces. Polynary Al-Si alloy hot etched. Optical. b Schematic representation of a. An included angle of 70.5° is formed by two intersected lines (111) and $(\bar{1}\bar{1}1)$. The numbers refer to measurements in Table 2. c Schematic representation of stem

silicon crystalline displaying a truncated octahedron, which evolves from a silicon octahedron nucleus, in initial stage of growth. d 3-D schematic representation of seed crystalline. The section of stem crystalline c on $(\bar{1}10)$ plane is shown by the thick lines

all crystallographic facets are exposed to the melt; 6 vertices and 11 edges are truncated; and 1 edge, at which (111) and $(11\bar{1})$ planes intersect, remains unchanged, leading to formation of 3 octagons, 2 heptagons, and 11 tetragons, respectively (Fig. 1d). Moreover, a new facet $(11\bar{2})$ appears and intersects with $(00\bar{1})$ and $(01\bar{1})$ (Fig. 1c), leaving 2 hexagons. Thus, 8 initial $\{111\}$ triangles are blunted to form 8 hexagons

(Fig. 1d) As a result, the grown irregular polyhedron in the first early stage is an equiaxed crystal in great degree with 48 vertices, 72 edges, and 26 facets being composed of 11 tetragons, 10 hexagons, 2 heptagons, and 3 octagons (Fig. 1b, d). The crystallographic characteristics of the deformed octahedron seem, in great degree, to be the crystal structure of potassium alum [26].

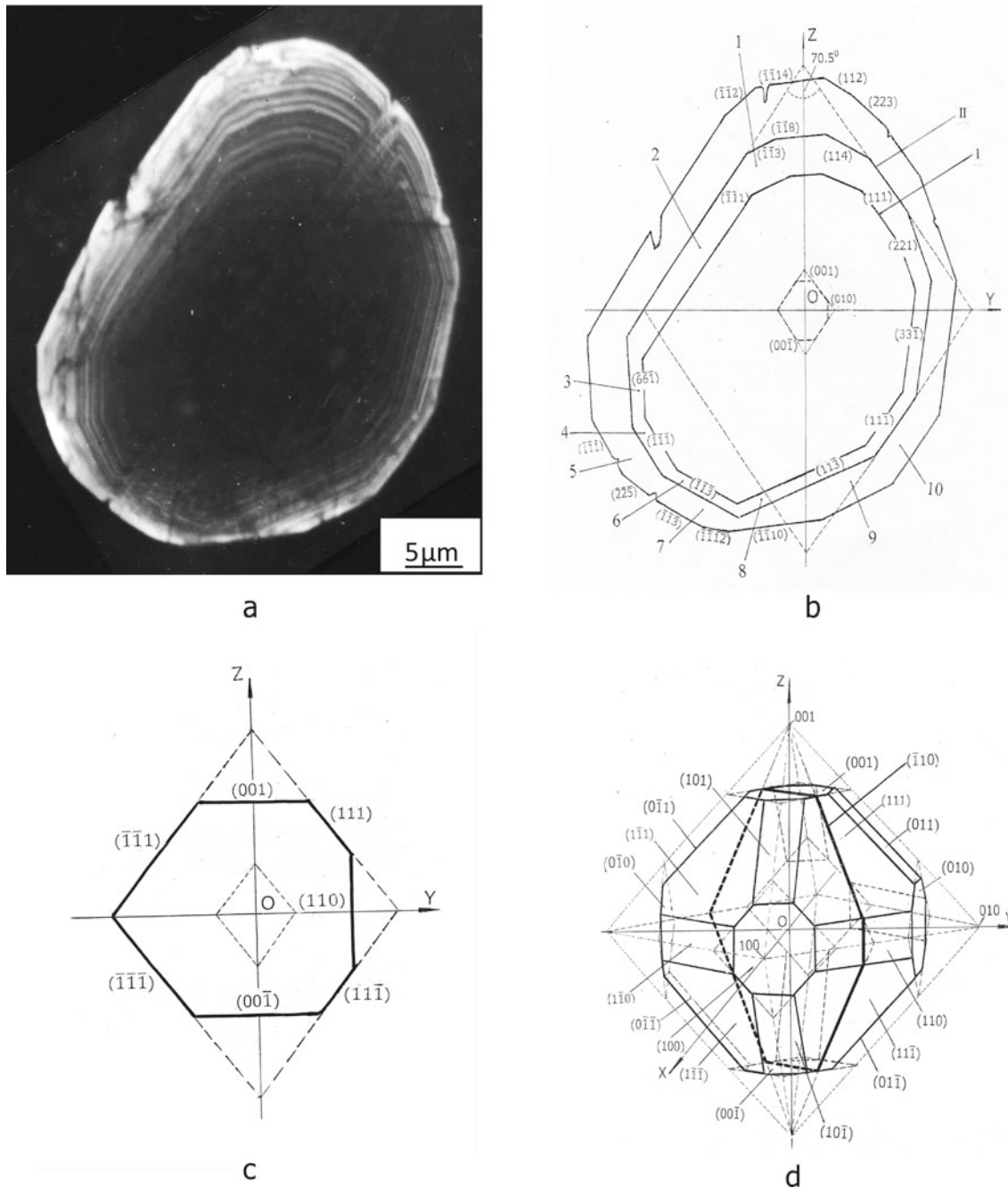


Fig. 2 **a** Microstructure of nodular silicon crystal exhibiting roundish outlines in the plan Section (110), with concentric layer growth traces parallel to external surface. Optical. **b** Schematic representation of **a**. Four dash lines intersected each other reveal an octahedral primary silicon crystal, from which roundish silicon developed. **c** Schematic

representation of stem crystal displaying a distorted octahedron in first early stage of silicon growth. **d** Stereo schematic representation of stem crystal showing a truncated octahedron. On $(\bar{1}10)$ plane the thick lines represent the section of stem crystal (**c**)

The microstructural characteristics of nodular silicon are similar to semi-nodular silicon although no growth trace is etched out in the central region. However outside this area the growth striations or layers clearly exhibit a series of the closed concentric traces parallel to the external periphery (Fig. 2a, b). It is very interesting that the growth layers are composed of

lots of high-indexed facets such as (221), (331), $(\bar{1}\bar{1}8)$, $(\bar{1}\bar{1}10)$, $(\bar{1}\bar{1}12)$, $(\bar{1}\bar{1}14)$, etc. making the silicon grain more roundish relative to semi-nodular silicon. Combining the experimental results in the semi-nodular silicon mentioned above, it would be expected that the silicon nodule will develop from a distorted octahedron in first early stage of

growth as shown by the dotted equiaxed configuration in Fig. 2b, c, and the nucleus would be an octahedron as shown in Fig. 2c. During initial growth of the octahedral nucleus, its 6 vertices and 11 ridges grow out, leaving 46 vertices, 69 ridges, and 25 facets being composed of 2 heptagons, 11 tetragons, and 12 octahedrons (Fig. 2d). The configuration can be recognized as an equiaxial blunted octahedron.

Concentric Layer Growth Stage

As growth proceeds, a silicon grain faced by different facets grows in such a concentric mode that the growth rate is almost identical in all orientations. Meanwhile, the growth morphology remains unchanged. However, some growth rates normal to two neighboring facets are not identical and a lot of edge angles of growth silicon particle are continuously truncated, forming new high-indexed facets. The new edge angle is much larger than the truncated angle, making the equiaxed crystal more roundish (Table 2). This growth characteristic different from the growth mode of octahedron [3] plays a determined role to develop the nodular silicon. It should be noted that whether the edge or corner grows downwards imposing the new facet is attributed to the difference of growth rate between two neighboring growth facets [3]. In our previous study [27], author developed an expression to predict the condition of stabilized faceted growth, as follows:

$$V_{[E]} = \left(V_{[abc]'} / \sin \alpha \right) \left\{ 1 + 2 \left(V_{[abc]} / V_{[abc]'} \right) \cos \alpha + \left(V_{[abc]} / V_{[abc]'} \right)^2 \right\}^{1/2} \quad (1)$$

where α is the angle (or ridge) between two neighboring growth traces, $V_{[E]}$ is growth rate of ridge or corner α , and $V_{[abc]}$ is growth rate normal to neighboring facet (abc) and (abc), respectively.

The general expression can be used to anticipate the limit of stable growth of crystal which is cut at random angles in microsection. If the expression (1) is satisfied for the growth rate of the ridge and two neighboring growth facets, the crystal will grow in stable mode, the crystal shape remaining intact. If $V_{[E]}$ is greater than the right-hand side (RHS), this represents accelerated corner growth and the corner grows outward. On the other hand, if $V_{[E]} < \text{RHS}$, corner growth is decelerated, and conditions favor the truncation of the corner or ridge to create a new facet.

Table 2 lists the variety of silicon morphology with the growth spaces measured on micro-sections accompanied with the corner (or ridge) α between 64.5 and 160.9° shown in Figs. 1 and 2. Figure 3 schematically demonstrates the relationship between grown morphology of silicon crystal and the

ratio of growth rate normal to two neighboring facets mentioned in Table 2. There are three growth modes describing the relationship. Firstly, growth spaces are of equal size, implying the same growth rate normal to different facets, either high or low index in certain interval during freezing. Equation (1) is satisfied as demonstrated by measurement numbers 1, 5, 8, 13, and 15 in Table 2 and Fig. 3. Silicon crystal grows homogeneously and this pattern is accurately reproduced with each successive growth trace. The growth mode can be referred to as “stable mode”. Observations demonstrate that most of the facets in nodular silicon grow in this mode. Secondly, a lot of growth rates normal to two neighboring facets are not of equal size with the ratio of growth velocity in range of $0.7 (\approx 1/\sqrt{2}) - 1.4 (\approx \sqrt{2})$ such as numbers 2, 6, 7, 9–12, and 17 in Table 2 and Fig. 3. In this case, the stable faceted growth tends to break down. However, these tendencies are usually quickly corrected, so that the faceted shape is recovered, and the expression is satisfied too. As a result, the growth profile is maintained unchanged; while the orientation and magnitude of the growth ridge change in a small degree (Figs. 1b and 2b). This mode of growth can be referred to as “sub-stable”. Thirdly, as $V_{[abc]}/V_{[abc]'} < 0.7 (\approx 1/\sqrt{2})$ or $V_{[abc]}/V_{[abc]'} > 1.4 (\approx \sqrt{2})$, $V_{[E]}$ is smaller than the right-hand side (RHS), thus the growth condition doesn't approach the requirement of Eq. (1). In this case, the growth of the ridge or corner decelerated, representing truncation of the ridge or corner with appearance of new higher indexed facets as shown by numbers 3, 4, 14, and 16 accompanied by the new edge angle larger than the truncated ridge angle (Table 2 and Fig. 3). This mode of growth would be referred to as “unstable mode”. It is apparent that truncation of the ridge or corner is an important step for the appearance of roundish silicon crystal.

The stability of growth morphology of nodular silicon crystal is attributed to the ratio of the growth rates normal to two neighboring facets. The greater the difference of growth rates normal to two neighboring facets, the worse the stability of growth morphology of silicon crystal. During the growth process the high-indexed facets continuously appear and the amount of facets on the external surface is increasing. However, the amount of facets on the external surface in semi-nodule (Table 3) is much less than in silicon nodule (Table 4), and therefore the silicon nodule (Fig. 2a) looks like a sphere in great degree compared with semi-nodule (Fig. 1a). Undoubtedly the silicon spherulite is a form developed from the stage of pyramid instability, exhibiting a multi-faceted crystal. In other words, nodular silicon is an equiaxed polyhedron bounded by fine facets with different index other than low-index one. This assumption is verified by the SEM observation on the silicon nodule, showing the hexagon and other polyhedrons on external surface (Fig. 4) (Tables 3 and 4).

Table 2 Average growth trace spacing measured in nodular silicon and the relationship with growth morphologic variety of silicon crystal

No.	Two neighboring growth facets ($V_{[abc]}$, $V_{[abc]'}$)	Measuring number A/ Measuring number B (in Figs. 1b, 2b)	Average growth space ($\text{mm} \times 10^{-3}$)			Growth space ratio ($V_{[abc]}/V_{[abc]'}$)	Included angle between $V_{[abc]}$ and $V_{[abc]'}$ (degree)	Limit of stable growth, RHSb ($\text{mm} \times 10^{-3}$)	V_E/RHS	Morphologic variety	Figure
			V_E	$V_{[abc]}$	$V_{[abc]'}$						
1	$V_{[11\bar{1}]}$, $V_{[111]}$	(6)/(4)	4.5	3.8	4.0	~ 1.0	109.5	4.6	~ 1	Stable growth	Figure 1b
2		(7)/(3)	2.5	2.2	1.8	1.3	109.5	2.5	1.0	Sub-stable growth	
3		(8)/(2)	1.2 ^a	0.8	2.0	0.4	109.5	2.0	0.6	New (010) appears. (111) shrinks. New 144.8 deg. ridge between (111) and (010) appears	
4	$V_{[001]}$, $V_{[111]}$	(20)/(4)	4.5 ^a	7.2	3.8	1.9	125.2	7.1	0.63	New (113) appears. New ridge between (113) and (111) is 150.7 deg	
5	$V_{[113]}$, $V_{[111]}$	(22)/(3)	2.6	2.0	2.0	1.0	150.7	2.5	1.0	Stable growth	
6	$V_{[001]}$, $V_{[\bar{1}\bar{1}\bar{1}]}$	(20)/(17)	7.0	7.2	5.0	1.4	125.2	7.2	~ 1	Sub-stable growth	
7		(21)/(18)	2.5	2.5	2.0	1.4	125.2	2.6	~ 1	Sub-stable growth	
8	$V_{[0\bar{1}0]}$, $V_{[\bar{1}\bar{1}3]}$	(16)/(13)	1.8	1.1	1.0	1.10	64.5	1.8	1.0	Stable growth	
9		(15)/(14)	2.0	1.0	1.5	0.7	64.5	2.2	0.9	Sub-stable growth	
10	$V_{[11\bar{2}]}$, $V_{[11\bar{1}]}$	(10)/(6)	4.0	3.5	3.0	1.2	160.9	3.9	~ 1	Sub-stable growth	
11		(11)/(7)	1.8	2.0	1.5	1.3	160.9	1.5	1.2	Sub-stable growth	
12	$V_{[\bar{1}\bar{1}3]}$, $V_{[\bar{1}\bar{1}1]}$	(1)/(2)	2.7	3.2	2.3	1.4	150.7	2.6	~ 1	Sub-stable growth	Figure 2b
13	$V_{[\bar{6}\bar{6}1]}$, $V_{[\bar{1}\bar{1}1]}$	(3)/(4)	1.5	1.1	1.2	0.9	151.6	1.4	1.1	Sub-stable growth	
14	$V_{[\bar{1}\bar{1}1]}$, $V_{[\bar{1}\bar{1}3]}$	(5)/(7)	2.5 ^a	3.0	2.0	1.5	150.7	3.3	0.76	New ($\bar{2}2\bar{5}$) appears. Ridge between ($\bar{1}\bar{1}1$) and ($\bar{2}2\bar{5}$) is 155 deg	
15	$V_{[\bar{1}\bar{1}3]}$, $V_{[11\bar{3}]}$	(6)/(8)	1.2	0.8	0.8	1.0	129.6	1.0	1.2	Stable growth	
16	$V_{[\bar{1}\bar{1}3]}$, $V_{[11\bar{3}]}$	(7)/(9)	1.1 ^a	2.0	2.8	0.7	129.6	3.2	0.34	New ($\bar{1}\bar{1}\bar{1}2$) and ($\bar{1}\bar{1}10$) appear. New 162 deg. ridge between ($\bar{1}\bar{1}3$) and ($\bar{1}\bar{1}\bar{1}2$) occurs. Ridge between ($\bar{1}\bar{1}3$) and ($\bar{1}\bar{1}10$) is 163 deg	
17	$V_{[11\bar{3}]}$, $V_{[11\bar{1}]}$	(9)/(10)	2.2	2.8	2.4	1.2	150.7	2.4	0.9	Sub-stable growth	

^aGrowth space of new facet is identified with the distance from ridge between two neighboring traces to the new facet

$$^b(V_{[abc]}/\sin\alpha) \{1 + 2(V_{[abc]}/V_{[abc]'})\cos\alpha + (V_{[abc]}/V_{[abc]'})^2\}^{1/2}$$

Discussion

When primary silicon crystal precipitates from melt the morphology of growing crystal is determined by the growth rate of interface of crystal in melt. As is well known the growth rate is dependent on the mechanism which controls

the rate of silicon atom attachment to the interface of silicon crystal. The controlling mechanism can be diffusion, at which the flux of atoms controls the growth rate, all atoms reaching the surface of silicon crystal being incorporated. In this case, the growth rates for all the facets would be the same as the diffusion rate of silicon atom in melt. Alternatively, the controlling mechanism can be crystallographic

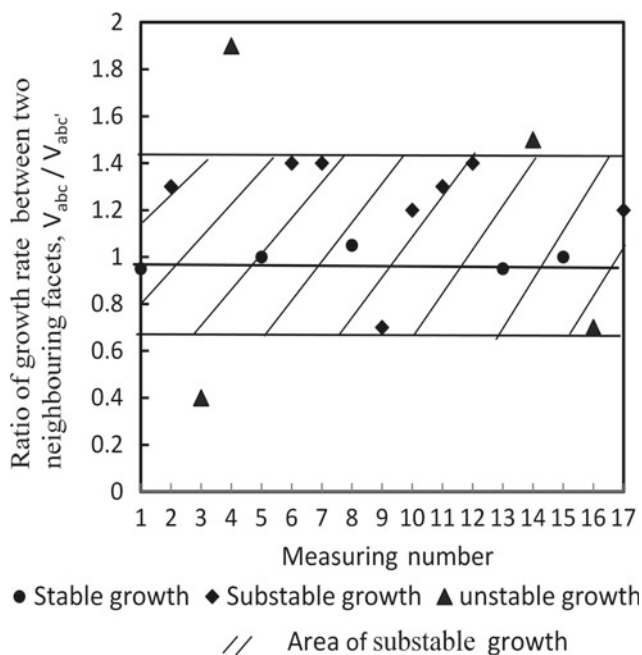


Fig. 3 The relationship between stability of growth of nodular silicon crystal and the ratio of the growth rates normal to two neighbouring facets. The measuring numbers refer to spacing measurements in Table 2

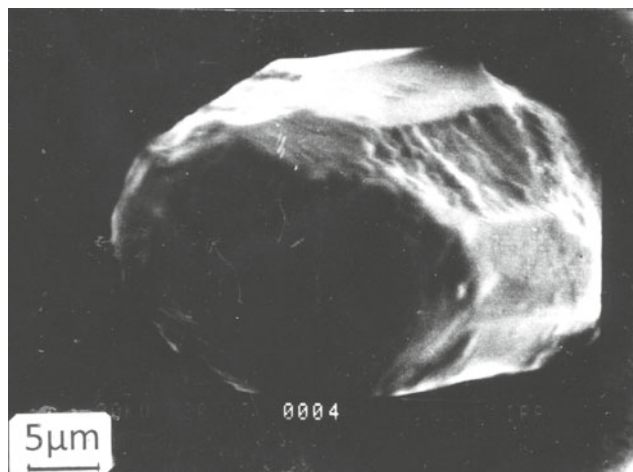


Fig. 4 SEM micrograph of silicon nodule, showing the hexagon and other polyhedrons on external surface

kinetics, in which the interface structure of silicon particle determines the rate in which atoms are accepted from the diffusion flux. Therefore, the kinetics growth rate is greatly affected by the roughness of the interfacial structure of crystal that depends on the structure of the crystal interface and the entropy of melting (δ_s/T_E), where δ_s is latent heat of melting and T_E is melting point. Jackson found that faceted growth is favored as a quantity $\alpha = (\delta_s/T_E)(N_S/N_V)$ exceeds

$2 \text{ cal/}^\circ\text{C}$, N_S and N_V are the number of close neighbors on the surface and within the body of a crystal, separately [28]. If quantity α is less than 2, a rough plane will grow up. The growth velocity on a facet plane seems to be much smaller than the rough plane [28]. In addition, the kinetics growth rate of higher index face is larger than low-index facets. Silicon is a boundary faceted crystal; its N_S and N_V vary with different planes, as shown in Table 5 and the growth rates normal to different facets are different. The value of 2.67 for silicon predicts that silicon should grow in faceted form with {111} favoured as the facet plane, however {110} and {100} with quantity α of less than 2 grow in nonfaceted mode. The growth velocity of the nonfaceted planes (100) and (110) is much greater than that of faceted (111) facet [28].

Temperature and solute field are two important factors influencing solute diffusion process and crystallization kinetics. According to the study of Jackson, the growth of primary silicon crystal in Al–Si alloy melt proceeds by a mechanism of dislocation spiral in the direction normal to a facet [21, 28]. The growth rate varies linearly or exponentially with the undercooling [28–30]. In contrast, the scale of the diffusion coefficient of aluminum and silicon in Al–Si alloy exponentially decreases when temperature drops down in melt, leading both diffusion rates to decrease [31–33].

At melting temperature, the kinetics growth rate is assumed to be zero. As freezing proceeds, the temperature of the melt continuously decreases to make the melt in undercooled state. As a result, both rates vary in opposite directions, accelerating the crystallization rate of silicon crystal and slowing down the diffusion rate of silicon in melt. Under small undercooling, for example, in the body of casting, the diffusion rate of silicon in melt might be greater than the kinetics growth rate of the lower index planes, for example, {111}, {110}, and {100}, but less than the kinetics growth rate of higher indexed facets, such as {113}, {331}, or {1114}, thus the growth rate of low-indexed facets {111}, {110}, and {100} is determined by their own kinetics growth rate. Moreover, the growth rate of facets (100) and (110) is larger than the growth rate of the plane (111) [28] and according to long held crystallographic rule [34] the higher growing planes grow out, leaving the slow-growing planes to form facets, finally causing the formation of almost perfect octahedral silicon bounded by eight {111} facets with strongly faceting. On or near the mould wall, the cooling rate of melt is much higher than in the body of casting, producing a larger undercooling [23], greatly enhancing these two tendencies mentioned above. As the silicon diffusion rate is much less than the kinetics growth rate of all planes, either higher index or lower, the growth velocities normal to all faces slow down and the growth rates of all facets are determined by the diffusion rate of silicon in

Table 3 Scheme of occurrence of new facet from nucleus to external surface in semi-nodular silicon crystal (Fig. 1b)

Initial stage	Stage of occurrence of new facet				
	I	II	III	IV	External surface
(111)	(001)	→(001)	→(001)	→(001)	→ $\bar{1}\bar{1}6$
		→(113)	→(113)	→(113)	→(112)
	(111)	→(111)	→(111)	→(111)	→(111)
				→(010)	→(010)
(11 $\bar{1}$)	(11 $\bar{1}$)	→(11 $\bar{1}$)	→(11 $\bar{1}$)	→(11 $\bar{1}$)	→(11 $\bar{1}$)
	(11 $\bar{2}$)	→(11 $\bar{2}$)	→(11 $\bar{2}$)	→(11 $\bar{2}$)	→ $\bar{2}\bar{2}3$
	(00 $\bar{1}$)	→(00 $\bar{1}$)	→(00 $\bar{1}$)	→(00 $\bar{1}$)	→(00 $\bar{1}$)
$(\bar{1}\bar{1}\bar{1})$	($\bar{1}\bar{1}\bar{1}$)	→($\bar{1}\bar{1}\bar{3}$)	→($\bar{1}\bar{1}\bar{3}$)	→($\bar{1}\bar{1}\bar{3}$)	→($\bar{1}\bar{1}\bar{3}$)
					→ $\bar{1}\bar{1}\bar{1}$
	(0 $\bar{1}$ 0)	→(0 $\bar{1}$ 0)	→(0 $\bar{1}$ 0)	→(0 $\bar{1}$ 0)	→(0 $\bar{1}$ 0)
$(\bar{1}\bar{1}1)$	($\bar{1}\bar{1}3$)	→($\bar{1}\bar{1}3$)	→($\bar{1}\bar{1}3$)	→($\bar{1}\bar{1}3$)	→($\bar{1}\bar{1}3$)
	(001)	→(001)	→(001)	→(001)	→ $\bar{1}\bar{1}6$
Amount of facets	8	9	9	10	11

melt. In this case, the formation of all facets is favored, providing the possibility of the formation of spherical silicon. The assumption has been demonstrated in our study. A few of small primary silicon nodules appeared near the boundary of chill casting. It is worth noting that if temperature and solute field surrounding the growing crystal is homogeneous, the contour of the crystal remains unchanged due to the same growth rate of all the facets. It is of importance that temperature and silicon gradients surrounding a growing crystal will rarely be spherically symmetrical due to the variety of silicon distribution and the latent heat evolved from silicon crystal during solidification. A local difference either in temperature or in the supersaturation of the melt can cause the differences of growth rate between adjacent facets, opening up possibility for occurrence of high-indexed facets as shown in Fig. 3. Considering the occurrence of nodular silicon with undercooling in melt [9–12], it would be safe to assume that the temperature field in current study is the most important factor affecting the crystal shape. During the development of fast-growing facet the larger amount of latent heat evolved from silicon per unit time significantly raises the temperature at the crystal-melt interface, accelerating the growth rate being compared with the adjacent slow-growing facet. In this case, a higher

growth velocity of edge or corner is required to satisfy the expression of Eq. (1) for the stable growth. However, the latent heat evolved from silicon is transferred into a larger volume of melt adjacent to a corner by comparison with the facet plane itself. Therefore, temperature rises by a smaller value in melt neighbouring a corner, resulting in lower growth velocity, ultimately favouring the truncation of the corner. At this stage, the atom arrangement will initially be distorted, and further atom additions to the blunted corner will tend to form other higher indexed crystallographic plane as shown in Table 2. The identity of the facet so formed would not be a chance event, when formed at an early stage of growth, such a lower indexed facet tends to be stable, as in the case of (010) and (113) in Fig. 2b and Table 3. On the other hand, at a late stage of growth, such higher indexed planes ($\bar{2}\bar{2}3$), ($\bar{1}\bar{1}10$), and ($\bar{1}\bar{1}14$) shown in Fig. 3b and Table 4 easily develop. It is obvious that the nodular silicon development can only be achieved by the lower silicon diffusion rate in high undercooled melt. This phenomenon is found in other references [9, 10] reporting that the morphology of silicon crystal in Al–Si alloys is function of undercooling in freezing. With rapid cooling the roundish crystal is easily formed from melt [35]. The spheroid silicon is an example of unstable growth in faceted systems.

Table 4 Scheme of occurrence of new facet from nucleus to external surface in nodular silicon crystal (Fig. 2b)

Nucleus (Fig.2b)	Initial stage	Stage of occurrence of new facet		
		I	II	External surface
(111)	(001)	($\bar{1}\bar{1}3$)	→($\bar{1}\bar{1}3$)	→($\bar{1}\bar{1}2$)
		($\bar{1}\bar{1}8$)	→($\bar{1}\bar{1}8$)	→($\bar{1}\bar{1}14$)
		(114)	→(114)	→(112)
				→(223)
	(111)	→(111)	→(111)	
(11 $\bar{1}$)	(010)	(221)	→(221)	→(221)
		(33 $\bar{1}$)	→(33 $\bar{1}$)	→(33 $\bar{1}$)
	(11 $\bar{1}$)	→(11 $\bar{1}$)	→(11 $\bar{1}$)	
$(\bar{1}\bar{1}\bar{1})$	(00 $\bar{1}$)	(11 $\bar{3}$)	→(11 $\bar{3}$)	→(11 $\bar{3}$)
				→($\bar{1}\bar{1}10$)
				→($\bar{1}\bar{1}12$)
	$(\bar{1}\bar{1}\bar{1})$	($\bar{1}\bar{1}\bar{3}$)	→($\bar{1}\bar{1}\bar{3}$)	→($\bar{1}\bar{1}\bar{3}$)
				→($\bar{2}\bar{2}\bar{5}$)
		($\bar{1}\bar{1}\bar{1}$)	→($\bar{1}\bar{1}\bar{1}$)	→($\bar{1}\bar{1}\bar{1}$)
	($\bar{6}\bar{6}\bar{1}$)	→($\bar{6}\bar{6}\bar{1}$)	→($\bar{6}\bar{6}\bar{1}$)	
$(\bar{1}\bar{1}\bar{1})$	$(\bar{1}\bar{1}\bar{1})$	($\bar{1}\bar{1}\bar{1}$)	→($\bar{1}\bar{1}\bar{1}$)	→($\bar{1}\bar{1}\bar{1}$)
		($\bar{1}\bar{1}\bar{3}$)	→($\bar{1}\bar{1}\bar{3}$)	→($\bar{1}\bar{1}\bar{2}$)
Amount of facets	7	12	12	16

Table 5 Jackson number α for silicon^a [27]

Plane	N_s/N_v	Quantity α cal/°C	Growth mode
{111}	3/4	2.67	Faceted growth
{100}	2/4	1.76	Nonfaceted growth
{110}	0.89	0.89	Nonfaceted growth

^aThe entropy of fusion is equal to 3.56 cal/°C

Conclusions

- (1) High cooling rate near the mould wall is the primary reason for causing the appearance of nodular silicon grain in the Al-14wt%Si alloy treated by the designed modifier consisting of P, Ti, B, and mischmetal (RE).
- (2) Nodular primary crystal silicon in hypereutectic Al-Si alloy is an unstable phase, with an equiaxed and finely

multi-faceted polyhedron bounded by different index facets.

- (3) Concentric layer growth is the growth mechanism of nodular silicon crystal.
- (4) The controlling mechanism for the development of silicon nodule crystal is Si diffusion in melt. Most of growth rates of different index facets are equal due to the equal diffusion rate of silicon atoms in melt surrounding crystal.

- (5) The growth rate difference in the range of $V_{abc}/V_{abc'} < 0.7$ ($\approx 1/\sqrt{2}$) or $V_{abc}/V_{abc'} > 1.4$ ($\approx \sqrt{2}$) between two adjacent facets, (abc) and (abc'), opening up the possibility for occurrence of high-indexed facets is the determining factor in developing a nodular silicon crystal

References

- J. Wang, Z. Guo, S.M. Xiong (2017) Characterization of the morphology of primary silicon particles using synchrotron X-ray tomography, *Materials Characterization*. 123: 354–359.
- J. Wang, Z. Gua, J.L. Song, W.X. Hu, J.C. Liu, S. M. Xiong (2018) On the growth mechanism of the primary particle in a hypereutectic Al-20 wt%Si alloy using synchrotron X-ray tomography. *Materials and Design*. 137: 176–183.
- R.Y. Wang, W.H. Lu, L.M. Hogan (1997) Faceted growth of silicon crystals in Al–Si alloys, *Metall. Mater. Trans. A*.28: 1233–1243.
- H. Singh, A.M. Gokhale, A. Tewari, S. Zhang, Y. Mao (2009) Three-dimensional visualization and quantization characterization of primary silicon particles in an Al–Si base alloy, *Scripta Materials*. 61: 441–444
- Wang, M. Wei, L.J. Zhang, Y. Du (2016) Morphologies of Primary Silicon in Hypereutectic Al–Si Alloys: Phase-Field Simulation Supported by Key Experiments. *Metall. Mater. Trans. A*. 47: 1510–1516.
- E. Schaberger-Zimmermann, M. Mathes, G. Zimmermann (2016) Hypereutectic Al–Si alloy gathering of 3D microstructure data. *JOM*. 68:2073–2081.
- K.V. Falch, D. Casari, M.D. Michiel, C. Detlefs, A. Snigireva, I. Snigireva, V. Honkimaki, R. H. Mathiesen (2017) In situ hard X-ray transmission microscopy for materials science. *J. Materials Sci*. 52: 3497–3507.
- H.S. Kang, W.Y. Yoon, K.H. Kim, M.H. Kim, E.P. Yoon (2004) Microstructure characterization of hypereutectic Al–Si alloys with different undercooling levels, *Mater. Sci. Forum*. 449–452: 169–172.
- H.S. Kang, W.Y. Yoon, K.H. Kim, M.H. Kim, E.P. Yoon (2005) Microstructure selections in the undercooled hypereutectic Al–Si alloys, *Mater. Sci. Engr*. 404A:117–123.
- R. P. Liu, D. M. Herlach, M. Vandyousefi, A. L. Greer (2004) Undercooling and solidification of Al-50 at.pct Si alloy by electromagnetic levitation. *Metall. Mater. Trans. A* 35: 607–612.
- K. Kuribayashi, K. Nagashio, Michio Tajima (2009) Spherical crystallization of Si during free fall in drop-tubes. *Journal of Crystal Growth*. 311:722–726.
- F.Y. Cao, Y.D. Jia, K.G. Prashanth, P. Ma, L.S. Liu, S. Scudino (2015) Evolution of microstructure and mechanical properties of as-cast Al–Si alloy. *Mater Design* 74: 150–156.
- J. Piątkowski, B. Gajdzik, T. Matuła (2011) Crystallization and structure of cast A390.0 Alloy with melt overheating temperature *Solid State Phenomena* 176:29–34.
- Xu, Y., Deng, Y., Casari, D. *et al* (2020) Revealing the nucleation kinetics of primary Si particles in hypereutectic Al–Si alloys under the influence of P inoculation. *J Mater Sci*. <https://doi.org/10.1007/s10853-020-05095-3>.
- A.G.C. Gwyer, H.W.L. Phillips (1926) The constitution and structure of the commercial aluminium-silicon alloys. *J. Inst. Metals*. 26:283–324.
- M.L.V. Gayler (1927) The undercooling of some aluminium alloys. *J. Inst. Metals* 38:157–194.
- R. Wladysiak, A. Kuzun (2015) Structure of Al-20Si Alloy in heat treated die casting. *Archieve of Foundry Engr*.15:113–118.
- N. Apaydin, R.W. Smith (1985) Microstructure characterization of rapidly solidified Al–Si alloys. *Mater. Sci. Engr*. 98A:149–152.
- M.G. Day (1968) Primary silicon spherulities in aluminum-silicon alloys, *Nature*. 219:1357–1358.
- J. Gruzleski, B. Closset (1990) *The Treatment of Liquid Aluminium-Silicon Alloys*. AFS, Inc. Des Plaines, Illinois, Chapter 7.
- R.Y. Wang, W.H. Lu, L.M. Hogan (1995) Twin related silicon crystals in Al–Si alloys and their growth mechanism. *Mat. Sci. Tech*. 11: 441–449.
- O.A. Astoy, F. Yilmaz, R. Elliott (1984) Growth structures in aluminium-silicon alloys. *J. Crystal Growth*. 66:137–146.
- B.B. Guliaev (1962) *Foundry process*, Machinery Publisher, Moscow p. 327–337, (in Russian).
- T.B. Abbott, B.A. Parker (1988) The origins of primary silicon particles in hypereutectic aluminum-silicon alloys. *Cast metals* 1:122–132.
- P.B. Crosley, L.F. Mondolfo (1966) The Modification of Aluminum-Silicon Alloys. *AFS Trans*. 74: 53–64.
- G.W. Chang, J.Z. Wang (2002) *Crystal growth and control in solidification of metal*. Metallurgical Industry Press. Beijing. p. 60. (In Chinese).
- R.Y. Wang, W.H. Lu, L.M. Hogan (1999) Growth morphology of primary silicon in cast Al–Si alloys and the mechanism of concentric growth. *Journal of Crystal Growth*, 207:43–54.
- K.M. Beatry, K.A. Jackson (2000) Monte Carlo modeling of silicon crystal growth, *Journal of Crystal Growth*, 211: 13–17.
- K.A. Jackson (1968) On the theory of crystal growth: growth of small crystals using periodic boundary conditions. *J. Crystal Growth*. 3, 4:507–517.
- D. Buta, M. Asta, J. J. Hoyt (2007) Kinetic coefficient of steps at the Si(111) crystal-melt interface from molecular dynamics simulations, *Journal of Chemical Physics*, 127. Article ID 074703.
- J.F. Shackelford (1994) *CRC Materials Sci. Eng. Handbook*. Second Ed., CRC Press. London. 236–247.
- I.F. Kolobnev (1964) *Heat Treatment of Aluminum Alloys*. Metallurgy Press. Moscow. p.47 (In Russian).
- J. Askill (1970) *Trace diffusion data for metals alloys and simple oxides*, Plenum Press. New York. p.43.
- C.W. Bunn and H. Emmett (1949) Crystal growth from solutions. 1. Layer formation on crystal faces. *Disc. Faraday Soc*. 5:19–132.
- C.B. Kim and R.W. Heine (1963–1964) *Fundamentals of Modification in the Aluminium-Silicon System*. *J. Inst. Mater*. 92:367–376.